Intelligent Automation & Soft Computing
DOI:10.32604/iasc.2022.023863
Article

Tech Science Press

Novel L2CL-LCL Topology for Wireless Power Transmission PMSM Powered Electrical Vehicle

Jenson Jose[1,*] and Jose P. Therattil[2]

[1]Department of EEE, Jyothi Engineering College, Thrissur, 679531, India
[2]Department of ECE, Jyothi Engineering College, Thrissur, 679531, India
*Corresponding Author: Jenson Jose. Email: jensonjosepapers678@gmail.com
Received: 24 September 2021; Accepted: 15 November 2021

Abstract: The Wireless Power Transmission (WPT) technology is a significant source of operation in the field of power transmission with tremendous potential in a wide range of applications. This paper proposes a novel strategy for L2CL-LCL topology, which comprises two capacitors and one inductor in the essential and one capacitor and one inductor in the auxiliary. Using MATLAB simulation, this paper compares the traditional DSLCL system and the proposed L2CL-LCL. The various parameters of this system are simulated. In the current system, input and output power are set to 200.1 and 182.4 W. The common framework's start to finish efficiency can be estimated as 90.10%. The input and output power for the proposed framework is 224.2 and 211.05 W. The proposed framework has a general efficiency of 95.2%, which is greater than the traditional system. The output of this topology is taken care of to an electric vehicle powered by Permanent Magnet Synchronous Motor. The efficiency of the electric vehicle gets improved to about 65.5%, which is better than the average efficiency of an electric vehicle. The various parameters of the electric vehicle are simulated. The experimental analysis also proves that the results provided closely resemble theoretical research, demonstrating the superiority of the proposed system.

Keywords: Power transmission; inductor; full-bridge inverter; electrical vehicle system; battery voltage

1 Introduction

Electrical energy assumes a crucial function for making human existence more helpful and agreeable. In many previous years, the transmission of electrical energy was done through wired networks. Nonetheless, the rise of utilizations like cell phones, electrically-controlled vehicles, space satellites, and biomedical implantable gadgets has required the need for exploration in Wireless Power Transfer (WPT) [1]. A compensation configuration is critical for a WPT framework since it decides the resonance frequency while limiting the power supply's volt-ampere rating, boosting coupling power transfer capacity, and accomplishing high efficiency [2–5].

Parallel-Parallel (PP), Parallel Series (PS), Series-Parallel (SP), and Series-Series (SS) are the four major compensation configurations [6]. PS and PP, which are parallel compensation topologies, are not suitable for a WPT. A voltage-source inverter lays a framework by generating large current spikes at switching transitions [7]. The adverse effects of powerless misalignment tolerance can be seen in SS and SP compensation topologies. As the coupling deteriorates, the input impedance decreases. When the coupling factor is set to zero, the input impedance is also set to zero. It is extremely harmful as the voltage source is short-circuited. As a result, SS and SP are not applicable, requiring a large separation between two coupling coils, such as dynamic electric vehicle (EVs) charging [8]. Commercializing wireless charging technology in electric vehicles is still a massive problem because of the need for high efficiency and power with a broad misalignment tolerance [9].

The Inductor-Capacitor-Inductor (LCL) was proposed to improve misalignment tolerance and avoid massive current spikes [10–14].

An upgraded multi-load solution for WPT that employs an LCC/S architecture to maintain load power steady. An architecture like this ensures that the power delivered to the loads is consistent. By incorporating the LCC topology into the primary side of the WPT system, the current flowing through the transmitting coil may be adjusted more easily. If the loads in the system fulfill specific limits, the system can function at maximum efficiency. It is crucial to undertake more study depending on the system's power requirement [15].

A double-sided LCL variable compensation topology with MCR-WPT (magnetically coupled resonance wireless power transfer system) is utilized for Constant current (CC) and Constant Voltage (CV) charging mode for an electric vehicle. The mathematical model is established for the double-sided LCL topology using a two-port network. The characteristics of CC and CV output modes are studied, respectively. In any case, the disadvantage is that the change of the framework input voltage can likewise influence the analysis results [16]. Tab. 1 shows the recent advancements in the field of compensation topologies used in WPT system.

Table 1: Literature survey table

Year	Authors	System	Structure	Specific
2020	Wu et al.	Wireless power transfer system (WPT)	Parity-Time-Symmetry (PT)	Multiple decoupled receiving coils for achieve high efficiency and power
2015	Hou et al.	Series/Series-Parallel compensator	Contactless power transfer (CPT)	Compensated Resonant Converter to achieve high efficiency and good output controllability
2009	Keeling et al.	LCL	LCL Inductive Power Transfer (IPT) pickup	Active tuning to maintain unity power factor in LCL
2015	Xin et al.	Inductive Power Transfer (IPT) system	Improved LCL resonant network	A series of improved topologies are proposed and compared
2014	Hao et al.	Inductive Power Transfer (IPT) system	Dynamic Model of LCL-T	Small-signal model of the power using the generalized state-space averaging technique
2020	Zhao et al.	MCR-WPT System	Double-sided LCL variable compensation topology	Specific parameter configuration method and compensation conversion
2019	Tan	Wireless power transfer system (WPT)	LCC/S topology	Improved multi-load system to keep the power received by the loads stable

The double-sided LCC (DS LCC) compensation configuration has been proposed to take care of the issues identified with bidirectional power transfer [17]. DS LCC has its load-independent operation frequency preferences, zero-voltage switching (ZVS), and zero phase angle (ZPA). [18] As it may, DS LCC needs two additional compensation capacitors, prompting expanded framework cost, and decreased power density [19]. The operation principle and a boundary-tuning technique were presented. Inconveniences of DS LCL are the low degree of freedom and irregular input current. High effectiveness and low VA rating are its focal points.

Efficiency is one of the obliges which impacts the performance of the WPT framework. The efficiency of WPT was the principal centre while building up a few compensation topologies. Regular DS LCL has an efficiency of 87.3% [20]. A novel parameter tuning technique is actualized in DS LCL [21] with a general efficiency of 90.2%. Efficiency based plan improvement of the double-sided LCL wireless power transfer framework is proposed [22] and, the overall efficiency of the optimized is 92.67% [23].

In recent years EVs have gained acceptance as the most feasible choice for helping to protect the environment while also attaining significant energy savings in transportation. The intelligent charging system can determine the device's location on its own, allowing for the efficient charging of the electric vehicle [24]. The key propulsion component in electric vehicles is the traction motor, which must have excellent power density and torque, a wide speed range, excellent performance, high dependability, and low distortion [25]. A hybrid control system improves the charging range and stability of electric vehicles under dynamic settings [26]. For EVs charging applications, L2CL-LCL Fig. 1a compensation is used in this work. A DC source, high-frequency inverter, L2CL-LCL compensating circuits, rectifier, and battery are all part of the EVs charging system shown in Fig. 1b. In high-performance drive systems like EVs, the Permanent Magnet Synchronous Motor (PMSM) has moved to the top among AC motors. PMSM has high torque-to-current rates, a high power-to-weight ratio, good performance, and ruggedness. Because of the advantages listed above, PMSMs are frequently employed in current variable speed AC drives, particularly in electric vehicle applications [27–30].

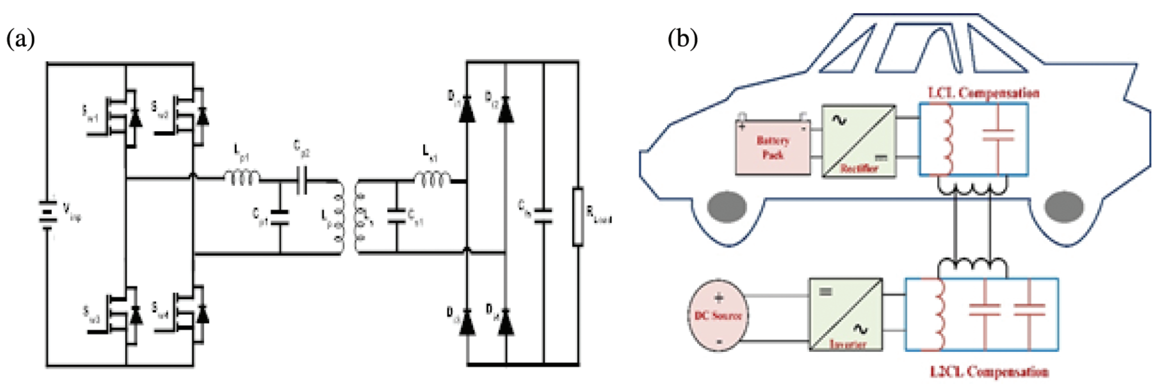

Figure 1: (a) Proposed circuit of the L2CL-LCL system, (b) wireless EV charging system

Due to its numerous advantages, PMSM is now often used in electric vehicles. The sinusoidal PWM with 180-degree variation controls the pulse to be sent to the switches in the inverter. The efficiency of an electric vehicle with a PMSM drive is in the range of 62%. The efficiency of the drive can be increased by up to 65.5% by using our topology.

2 Conventional Parameter Turning Method of Proposed L2CL-LCL System and Modeling of PMSM

Fig. 1 presents the circuit diagram of a proposed L2CL-LCL device. S_{w1}–S_{w4} are four MOSFETs that make up a Full-Bridge Inverter, and U_{inp} is the initial input DC voltage. The switch pairs (S_{w1}, Sw_4) and (S_{w2}, Sw_3) conduct in turn. L_{p1}, C_{p1} and C_{p2}, are the primary compensated inductors and capacitors. L_{s1} and C_{s1} are the secondary elements that correspond to each other. The analytical circuit of the proposed L2CL-LCL framework is as appeared in Fig. 2. For investigation purposes, the filter capacitor, load resistance and the diode rectifier circuit in Fig. 2 is replaced by its equivalent resistance $R_{ELoad.}$

$$RE_{Load} = \frac{8}{\pi^2} R_{Load} \tag{1}$$

R_{ELoad} can still be computed, as per reference [31].

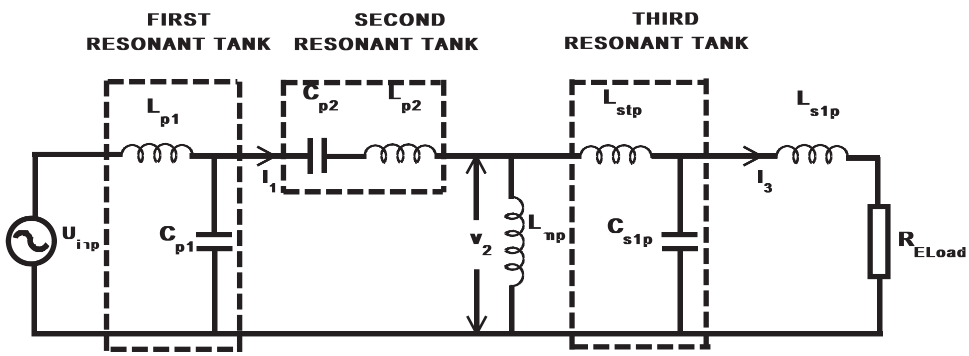

Figure 2: L2CL-LCL framework analytical circuit

The following basic equations are derived using the fundamental circuit concept [21].

$$L_{mp} = kL_p$$

$$L_{pt} = L_p(1-k) = L_{stp}$$

$$C_{s1p} = \frac{L_p}{L_s} C_{s1}$$

$$L_{S1P} = \frac{L_s^2}{L_p}$$

$$R_{ep} = \frac{8L_p R_{Load}}{\pi^2 L_s} \tag{2}$$

Consider the dotted line in Fig. 2 which depicts three resonant circuits. A first resonant tank is formed when L_{p1} and C_{p1} resonate at the device operating frequency. Similarly, C_{p2}, L_{p2} and L_{stp}, C_{s1p} make up the second and third resonant tanks.

These three resonant tanks resonate at the same system operating frequency ω_0 [32,33].

$$\omega_0^2 = \frac{1}{L_{p1} C_{p1}} = \frac{1}{L_{pt}\, C_{p2}} = \frac{1}{L_{stp}\, C_{s1p}} \tag{3}$$

Kirchhoff's current and voltage law can be used to determine the output current of the first resonant tank,

$$I_1 = \frac{U_{inp}}{j\left(X_{Lp1} - X_{Cp1}\right)} = \frac{-jU_{inp}}{\sqrt{L_{p1}^2\omega_0^2 + \frac{1}{C_{p1}^2 + \omega_0^2}}} \tag{4}$$

Substituting Eq. (3) in Eq. (4)

$$I_1 = \frac{-jU_{inp}}{\sqrt{2}}\sqrt{\frac{C_{p1}}{L_{p1}}} \tag{5}$$

Let I_2 be the second resonant tank's output current and V_2 be the voltage across it.

$$I_2 = \frac{V_2}{Z}$$

$$V_2 = I_1 j\sqrt{X_{Lp1}{}^2 + X_{Cp2}{}^2} \tag{6}$$

Substituting the Eq. (5) in Eq. (6) and rearranging

$$V_2 = U_{inp}\sqrt{\frac{C_{p1}L_{pt}}{L_{p1}C_{p2}}} \tag{7}$$

Let I_3 be the output current of the second resonant tank

$$I_3 = \frac{V_2}{jX_3} = \frac{U_{inp}\sqrt{\frac{C_{p1}L_{pt}}{L_{p1}C_{p2}}}}{j\sqrt{L_{stp}^2\omega_0^2 + \frac{1}{C_{s1p}^2\omega_0^2}}} \tag{8}$$

Divide and Multiply L_{p1} and L_{p2} and substituting Eq. (3) into Eq. (8) I_3 can be simplified as

$$I_3 = \frac{-jU_{inp}}{\sqrt{2}\,\omega_0 L_{p1}} \tag{9}$$

The average Power consumed by RE_{Load} is

$$P_{RELoad} = \frac{8U_{inp}^2 L_p\, R_{ELoad}}{2\pi^2\omega_0^2\, L_{p1}^2\, L_s} \tag{10}$$

R_{ELoad} consumes the Power specified in Eq. (10). Derived the current flowing through R_{ELoad} as per the energy conservation principle as

$$P_{RELoad} = I_{RELoad}^2 R_{ELoad}$$

Substituting the value of P_{RELoad}, after rearranging

$$I_{RELoad} = \frac{2U_{inp}}{\pi\omega_0 L_{p1}}\sqrt{\frac{L_p}{L_s}} \tag{11}$$

Different parameters are rearranged as

$$L_{p1} = \frac{2V_{ab}}{\pi\omega_0 I_{RELoad}}\sqrt{\frac{L_p}{L_s}} \tag{12}$$

$$C_{p1} = \frac{\pi I_{RELoad}}{2V_{ab}\omega_0}\sqrt{\frac{L_p}{L_s}} \tag{13}$$

$$C_{p2} = \frac{1}{\omega_0^2 L_p(1-k)} \tag{14}$$

$$C_{s1} = \frac{L_s}{\omega_0^2 L_p^2(1-k)} \tag{15}$$

The Eqs. (12)–(15) are used to calculate the values of the passive elements. Tab. 2 lists the designed values of the novel L2CL-LCL parameters.

Table 2: Designed values of the novel L2CL-LCL parameters

Parameters	Values
L_{p1}	67.43 μF
C_{p1}	52.13 nF
C_{p2}	14.33 nF
C_{s1}	14.33 nF
C_{fs}	220 μF

2.1 Modelling of PMSM Motor

A permanent magnet's back EMF generated by an energized coil is identical. Consequently, a PMSM has a mathematical model similar to the wound rotor Synchronous motor. The rotor frame was chosen because the instantaneous induced EMFs are determined by the orientation of the rotor magnets. The following assumptions are taken into consideration in the derivation.

- The induced EMF is sinusoidal; hence the stator windings are balanced, so saturation and parameter variations are ignored.
- Eddy current and hysteresis losses are close to zero.
- In the field, there are no current dynamics.
- On the rotor, there is no enclosure.

The motor's electromagnetic torque is calculated as follows:

$$T = \frac{3}{2}\frac{P}{2}\left\{\lambda_{ds}^r i_{qs}^r - \lambda_{qs}^r i_{ds}^r\right\} \tag{16}$$

The voltage equations for three-phase stators are as follows

$$V_{as} = V_m \sin \omega t \tag{17}$$

$$V_{bs} = V_m \sin\left(\omega t - \frac{2\pi}{3}\right) \tag{18}$$

$$V_{cs} = V_m \sin\left(\omega t - \frac{2\pi}{3}\right) \tag{19}$$

V_{as}, V_{bs}, V_{cs}—Stator phase voltages

V_m—Stator peak voltage

ω—Synchronous speed in rad/s

Park's transformation is used to convert the stator voltages in the 'abc' axis Vabc to the d, q axes

$$V_{qdo}.V_{qdos} = K_s V_{abcs} \tag{20}$$

$$K_s = \frac{2}{3}\begin{bmatrix} \cos\theta & \cos\left(\theta - \frac{2\pi}{3}\right) & \cos\left(\theta + \frac{2\pi}{3}\right) \\ \sin\theta & \sin\left(\theta - \frac{2\pi}{3}\right) & \sin\left(\theta + \frac{2\pi}{3}\right) \\ \frac{1}{2} & \frac{1}{2} & \frac{1}{2} \end{bmatrix} \tag{21}$$

$$\begin{bmatrix} V_{ds} \\ V_{qs} \\ V_{os} \end{bmatrix} = \frac{2}{3}\begin{bmatrix} \cos\theta & \cos\left(\theta - \frac{2\pi}{3}\right) & \cos\left(\theta + \frac{2\pi}{3}\right) \\ \sin\theta & \sin\left(\theta - \frac{2\pi}{3}\right) & \sin\left(\theta + \frac{2\pi}{3}\right) \\ \frac{1}{2} & \frac{1}{2} & \frac{1}{2} \end{bmatrix}\begin{bmatrix} V_{as} \\ V_{bs} \\ V_{cs} \end{bmatrix} \tag{22}$$

θ is a rotor angle.

Eqs. (23) and (24) give the stator current in a synchronously rotating reference frame

$$i^e_{qs} = \int \frac{V^e_{qs}}{L_q} - \omega_e \frac{\lambda_{af}}{L_q} - \frac{R_s}{L_q} i^e_{qs} - \omega_e i^e_{ds} \frac{L_d}{L_q} \tag{23}$$

$$i^e_{ds} = \int \frac{V^e_{ds}}{L_d} - \frac{R_s}{L_q} i^e_{ds} - \omega_e i^e_{qs} \frac{L_q}{L_d} \tag{24}$$

i^e_{ds}, i^e_{qs}—Current at d and q axis in reference frame of synchronous rotating.

V^e_{ds}, V^e_{qs}—Voltage at d and q axis in reference frame of synchronous rotating.

In terms of inductances and current, Eq. (25) gives the electromagnetic torque produced by the motor.

$$T = \frac{3}{2}\frac{P}{2}\left\{\lambda_{af} i^e_{qs} + \left(L_d - L_q\right) i^e_{qs} i^e_{ds}\right\} \tag{25}$$

The relation between the load torque and electromagnetic torque is given by

$$T_e = T_L + B\omega_m + J\frac{d\omega_m}{dt} \tag{26}$$

P—Number of pole pairs; B—Damping coefficient; T_L—Load torque; J—moment of inertia; ω_m—Rotor speed.

Rotor mechanical speed ω_m is provided by

$$\omega_m = \frac{1}{J}\int T_e - T_L - B\omega_m \tag{27}$$

Rotor electrical speed ω_e is provided by

$$\omega_e = \frac{P}{2}\omega_m \tag{28}$$

Rotor angle θ_m is given by

$$\theta_m = \omega_m \tag{29}$$

The PMSM-powered electrical vehicle system is depicted in block diagram form in Fig. 3. An inverter receives the battery's output. The PMSM is aided in driving the electric car by the AC supply provided by the inverter.

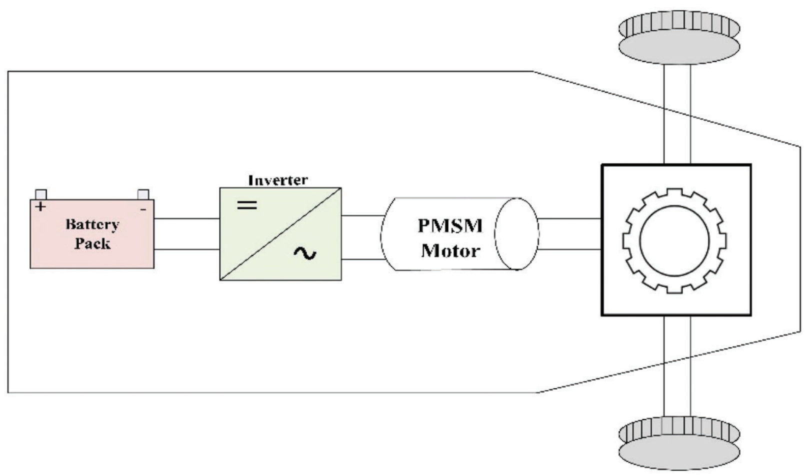

Figure 3: Block diagram of the PMSM powered electrical vehicle system

3 Design Example and Simulation Outcomes of Proposed System

Tab. 3 shows the objective system's simple presentation files. The rectifier diodes and inverter MOSFETs are the same as in the standard DS-LCL setup.

Table 3: The primary system's critical performance measures

Symbol	Parameter	Values
U_{inp}	Input DC Voltage	300 V
F	Frequency of Entire System	85 kHz
IR_{Load}	System Output Current	1 A
PR_{Load}	Rated Output Power	200 W

The output simulation considering various parameters and the tabulation for the proposed system is given. By varying various parameters, the output power *vs*. time is plotted in Fig. 4.

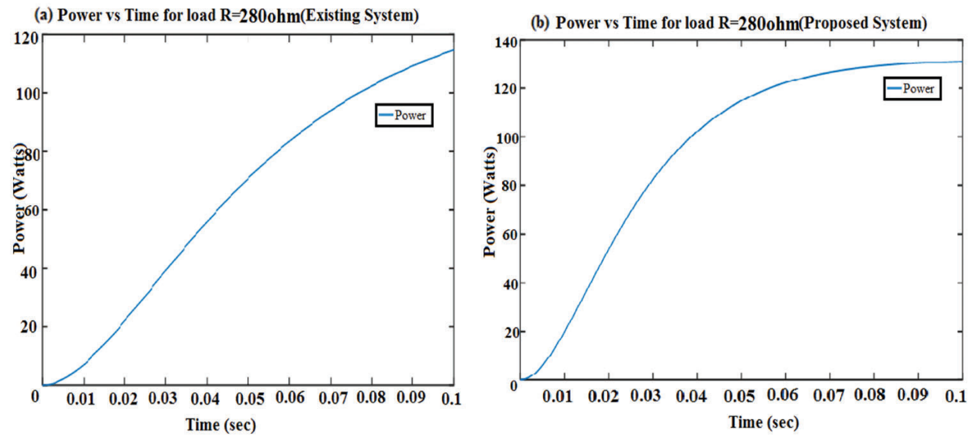

Figure 4: Output power *vs*. time waveform for load R = 280 ohm. (a) Traditional DS-LCL framework, (b) L2CL-LCL framework

When the resistance of the circuit gets increased compared to the original value, the current in the circuit gets reduced and voltage gets increased. The graph shows that the output power and efficiency have been increased by 21.9% (approximately 22%) and 3.2% respectively, compared to the traditional DS-LCL system.

When the resistance of the circuit gets reduced compared to the original value, the current and Power gets increased. From the graph, we can observe that the output power and efficiency have been increased by 14% and 0.4% respectively, compared to the traditional DS-LCL system. Tab. 4 shows the comparison result for various resistor values of the traditional and proposed system and the comparison values of the proposed and the traditional system for various capacitance values in Tab. 5.

Table 4: Comparison values for the L2CL-LCL and DS-LCL system

Parameter	R = 300 Ω		R = 280 Ω	
	DS-LCL	L2CL-LCL	DS-LCL	L2CL-LCL
Output Voltage	185.3	204.6	179.2	191.1
Output Power	140	160.1	114.7	110.0
Efficiency	92.6	95.8	92.7	95.2

Table 5: Comparison values of the proposed and the traditional system for various capacitance values

	C_1 = 104 nf; C_2 = 43 nf		C_1 = 103.8 nf; C_2 = 42.8 nf	
Parameter	DS-LCL	L2CL-LCL	DS-LCL	L2CL-LCL
Output Voltage	163.7	200.9	160.6	204
Output power	96.7	144.2	92.11	148.6
Efficiency	64	89	59.45	92.8

Fig. 5 compares two types of special compensations, DS-LCL and DS-LCC compensations, with the L2CL-LCL compensation. It is seen that the efficiency of the system is obtained as 95.03% which is better than the other two compensations, where DS-LCC has 93.1% and DS-LCL has 92.8%. It is seen that the efficiency of the system is obtained as 95.03% which is better than the other two compensations, where DS-LCC has 93.1% and DS-LCL has 92.8%.

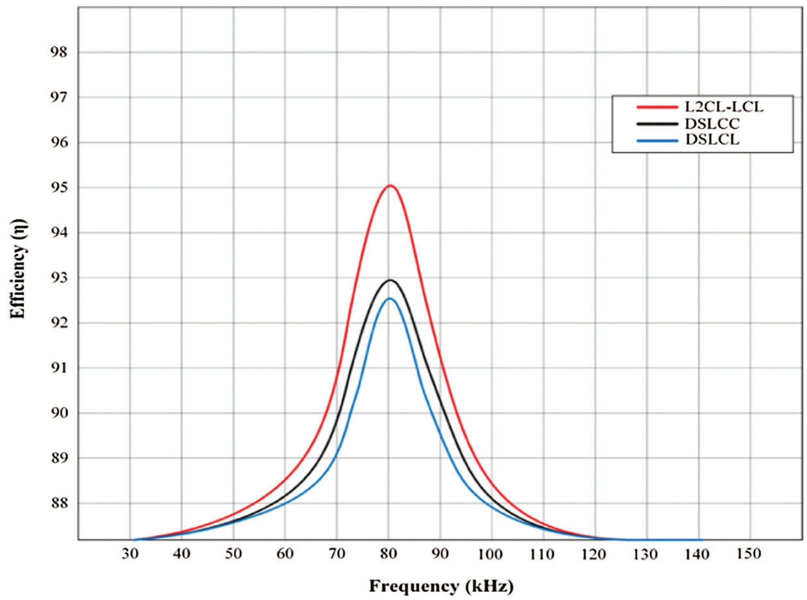

Figure 5: Efficiency *vs*. frequency at different compensation topologies

Fig. 6 demonstrates that efficiency is proportional to the coefficient of coupling and frequency. The smaller the air spaces, the better efficiency. For maximum power transfer, it is critical to strike a balance between distance and efficiency while keeping the application in the account and the efficiencies of various rated power ratings with various misalignments are shown in Fig. 7. The efficiency of the aligned system decreases as the rated output power decreases, whereas the misaligned system's efficiency is better than the aligned system's at the same lower-rated Power.

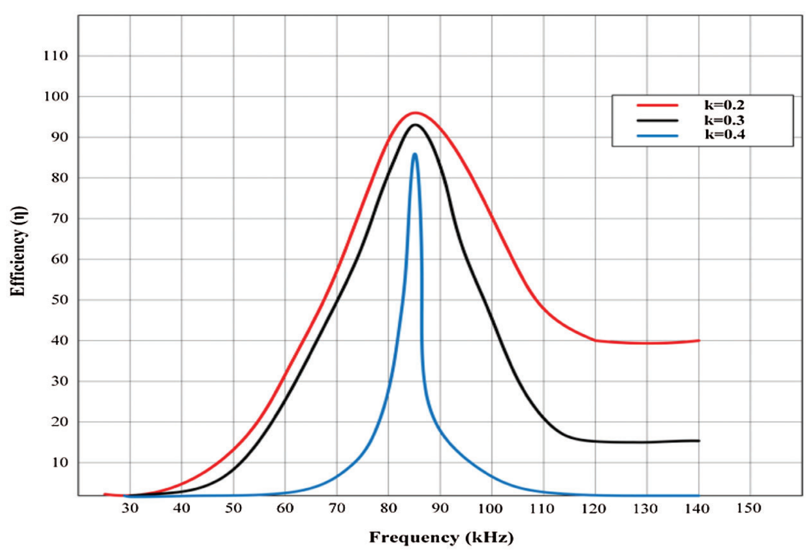

Figure 6: Efficiency *vs*. frequency at different coupling coefficients

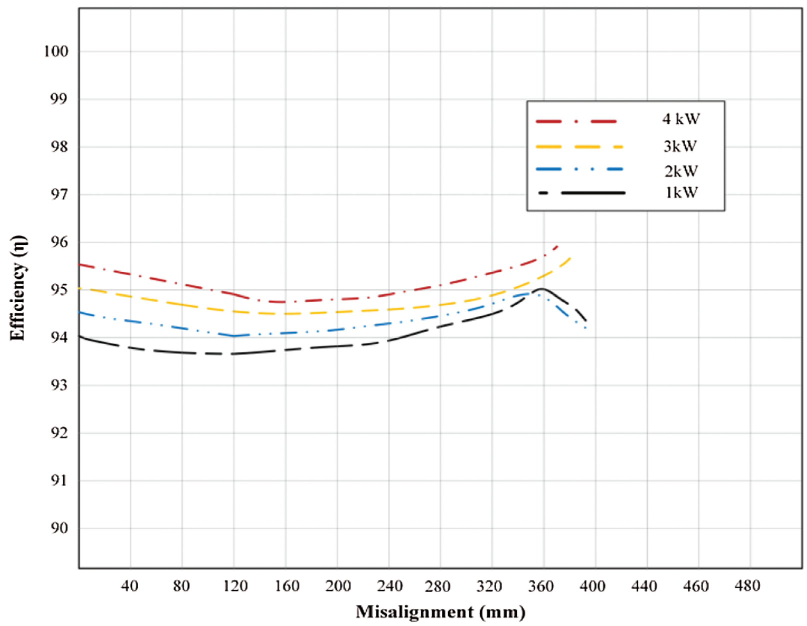

Figure 7: Efficiencies of various rated power ratings with various misalignments

Fig. 8 shows the simulation results for various coupling coefficients, input voltages, and output voltages under various battery voltage. For varying coupling coefficients and output voltages, the output power fluctuates linearly with the input voltages. Different coupling coefficients can be achieved by altering the spacing and misalignment between the receiver and transmitter coils.

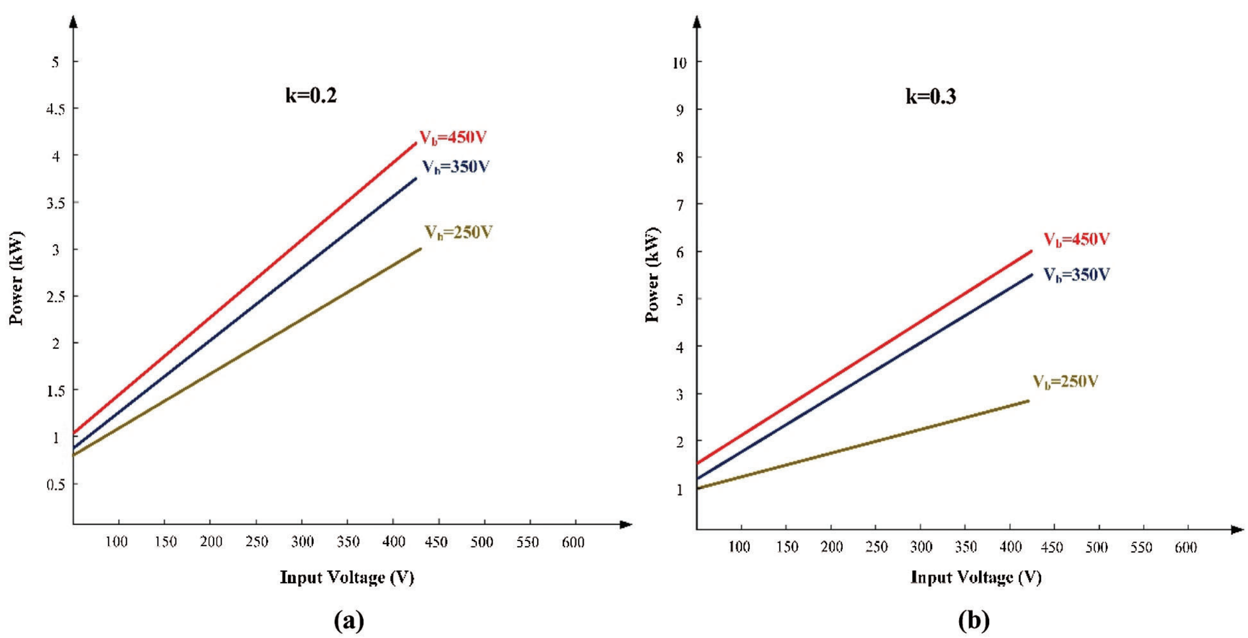

Figure 8: Simulation results for the L2CL-LCL system's power levels (a) k = 0.2 (b) k = 0.3

4 Experimental Validation

Fig. 9 displays the hardware setup of the proposed system. It consists of Digital Storage Oscilloscope, Rheostat, Permanent Magnet Synchronous Motor, Load, Auto transformer and Field Programmable Gate Array (FPGA) controller. The output wave forms produced from the hardware setup is provided below. Fig. 10 shows the back EMF waveform of PMSM. Back EMF is a voltage developed by the motor's rotation. As PMSM requires the AC supply, the back EMF generated in PMSM will be sinusoidal. Here the back EMF generated will be approximately equal to 20 V.

Figure 9: Hardware setup of the L2CL-LCL with PMSM

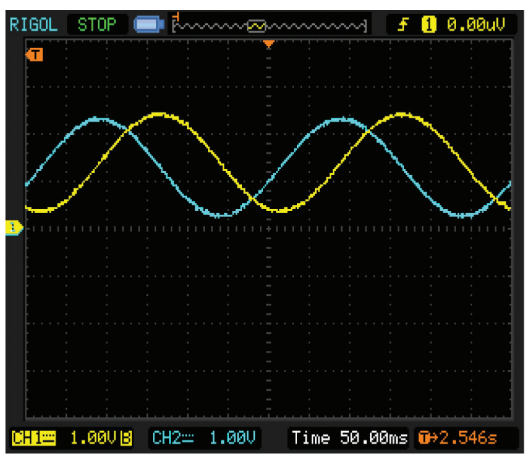

Figure 10: Back EMF waveform of the PMSM

The input DC voltage provided to the inverter and its value is equal to 300 V and the Fig. 11 shows the PWM pulse waveform. These waveforms are used to control the pulse which is given to the switches in the inverter. The technique used to control the pulse is the Sinusoidal PWM technique. Finally, Fig. 12 shows the speed waveform of the motor. The yellow line indicates the reference speed of the motor, which is equal to 1500 rpm and the green line indicates the motor's actual speed.

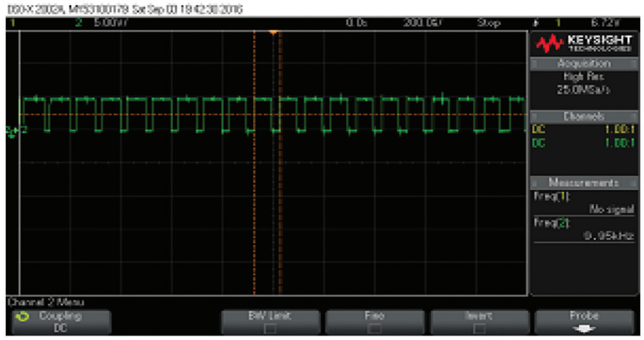

Figure 11: PWM pulse waveform

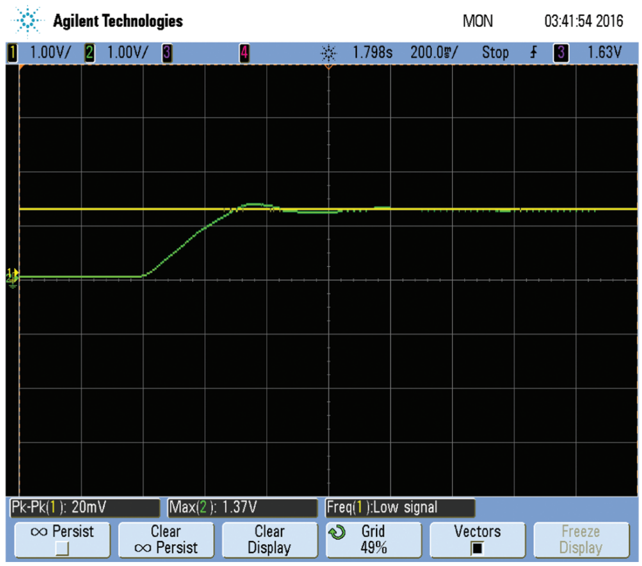

Figure 12: Speed waveform of the motor

Fig. 13 shows the variation of set voltage and actual voltage. The yellow line indicates the reference voltage and the blue line indicates the actual voltage. The speed begins to vary at the time of 5 s and settles at the time of 7 s. Fig. 14 shows the waveform of actual torque and reference torque. Again, the blue line indicates the yellow line indicates the torque and the reference torque. The dip in the waveform occurs due to the load variation.

Fig. 15 indicates the waveform of Voltage Source Inverter (VSI) output after providing filter. The Output from VSI will be fed to the PMSM. Tab. 6 shows the comparison of efficiency obtained during the simulation and hardware results and he performance comparison of wireless power transfer methods were tabulated in Tab. 7.

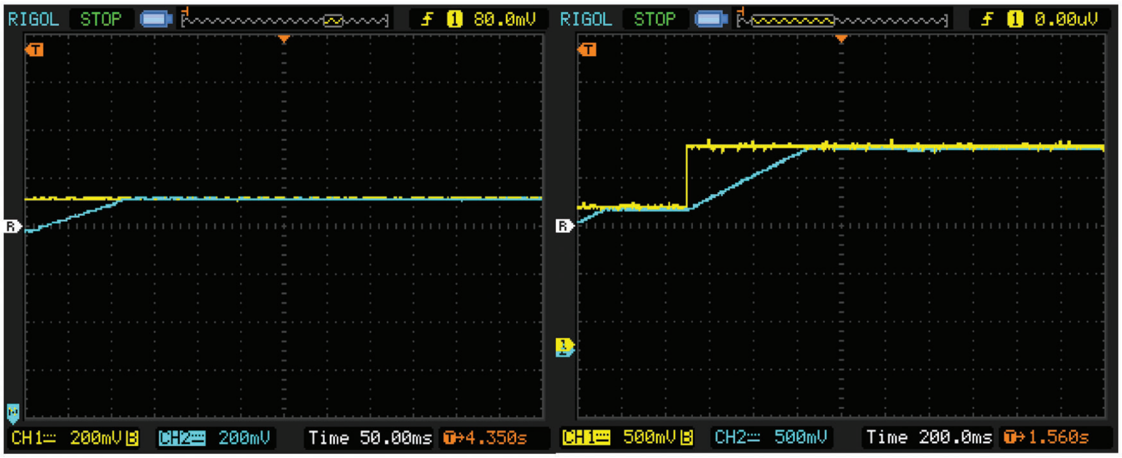

Figure 13: Set DC voltage and actual voltage

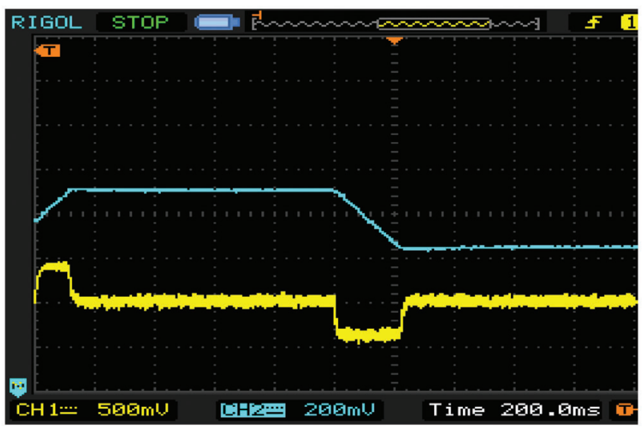

Figure 14: Actual torque and the reference torque

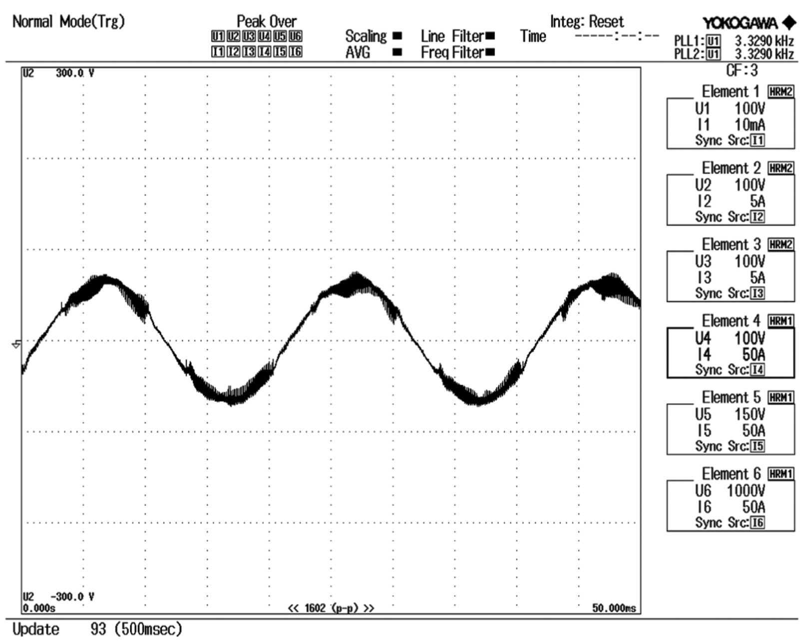

Figure 15: VSI output after filter

Table 6: Comparison of efficiency values

Parameters	Simulation	Hardware
Input Voltage	220	220
Output Voltage	144.1	137.3
Efficiency	65.5	62.4

Table 7: Performance comparison of wireless power transfer methods

WPT methods	Comparison parameters				
	Output power	Distance	Cost	Efficiency	Biological effects
Magnetic Resonance	60 W	Few Meters	Inexpensive	Upto 45%	No harmful effects
Microwave	100 kW	Few Kilometers	Expensive	Upto 54%	Damages Living issue
Laser	Several hundred Kilowats	Few Kilometers	Expensive	Upto 30%	Damages Living tissue

5 Conclusion

A new L2CL-LCL compensation topology is proposed in this paper. MATLAB simulation is also used to compare the traditional DSLCL system with the proposed L2CL-LCL structure. This topology produces an efficiency of about 95.2% which is better than the traditional system. The input and output power for the conventional framework is 200.1 and 182.4 W respectively. The conventional DSLCL framework's efficiency is measured as 90.10%. The input and output power for the proposed system is 224.2 and 211.05 W. The efficiencies of various topologies with output power are also tabulated. The output of this topology is fed to an electric vehicle driven by PMSM. The efficiency of the electric vehicle gets improved to about 65.5% which is better than the average efficiency of an electric vehicle. The various parameters of EVs are simulated and results are produced. The experimental analysis results from the theoretical analysis by proving the recommended system's efficiency is improved.

Acknowledgement: The authors would like to thank APJ Abdul Kalam Technological University and also we like to thank Anonymous reviewers for their so-called insights.

Funding Statement: The authors received no specific funding for this study.

Conflicts of Interest: The authors declare that they have no conflicts of interest to report regarding the present study.

References

[1] Y. Li, J. Hu, X. Li, F. Chen, Q. Xu *et al.,* "Analysis, design, and experimental verification of a mixed high-order compensations-based WPT system with constant current outputs for driving multistring LEDs," *IEEE Transactions on Industrial Electronics*, vol. 67, no. 1, pp. 203–213, 2019.

[2] W. Zhang, S. C. Wong, K. T. Chi and Q. Chen, "Design for efficiency optimization and voltage controllability of series-series compensated inductive power transfer systems," *IEEE Transactions on Power Electronics*, vol. 29, no. 1, pp. 191–200, 2013.

[3] H. H. Wu, A. Gilchrist, K. D. Sealy and D. Bronson, “A high efficiency 5 kW inductive charger for EVs using dual side control,” *IEEE Transactions on Industrial Informatics*, vol. 8, no. 3, pp. 585–595, 2012.

[4] A. J. Moradewicz and M. P. Kazmierkowski, “Contactless energy transfer system with FPGA-controlled resonant converter,” *IEEE Transactions on Industrial Electronics*, vol. 57, no. 9, pp. 3181–3190, 2010.

[5] W. Zhang, S. C. Wong, K. T. Chi and Q. Chen, “Design for efficiency optimization and voltage controllability of series-series compensated inductive power transfer systems,” *IEEE Transactions on Power Electronics*, vol. 29, no. 1, pp. 191–200, 2013.

[6] W. Zhang, S. C. Wong, C. K. Tse and Q. Chen, “Design for efficiency optimization and voltage controllability of series-series compensated inductive power transfer systems,” *IEEE Transactions on Power Electronics*, vol. 29, no. 1, pp. 191–200, 2014.

[7] W. Zhang and C. C. Mi, “Compensation topologies of high-power wireless power transfer systems,” *IEEE Transactions on Vehicular Technology*, vol. 65, no. 6, pp. 4768–4778, 2016.

[8] A. A. S. Mohamed, A. Berzoy, F. G. N. D. Almeidas and O. Mohammed, “Modeling and assessment analysis of various compensation topologies in bidirectional IWPT system for EV applications,” *IEEE Transactions on Industry Applications*, vol. 53, no. 5, pp. 4973–4984, 2017.

[9] L. Zhao, D. J. Thrimawithana and U. K. Madawala, “A comparison of LCL and LC bi-directional inductive power transfer systems,” in *Proc. Int. Power Electronics and Application Conf. and Exposition*, Shanghai, China, pp. 766–771, 2014.

[10] L. Wu, B. Zhang and J. Zhou, “Efficiency improvement of the parity-time-symmetric wireless power transfer system for electric vehicle charging,” *IEEE Transactions on Power Electronics*, vol. 35, no. 11, pp. 12497–12508, 2020.

[11] J. Hou, Q. Chen, S. C. Wong, K. T. Chi and X. Ruan, “Analysis and control of series/series-parallel compensated resonant converter for contactless power transfer,” *IEEE Journal of Emerging and Selected Topics in Power Electronics*, vol. 3, no. 1, pp. 124–136, 2014.

[12] N. Keeling, G. A. Covic, F. Hao, L. George and J. T. Boys, “Variable tuning in LCL compensated contactless power transfer pickups,” in *Proc. IEEE Energy Conversion Congress and Exposition*, San Jose, CA, USA, pp. 1826–1832, 2009.

[13] D. Xin, L. Weiyi, L. Yanling, S. Yugang, T. Chunsen *et al.,* “Improved LCL resonant network for inductive power transfer system,” in *Proc. IEEE PELS Workshop on Emerging Technologies: Wireless Power*, Daejeon, Korea (South), pp. 1–5, 2015.

[14] H. Hao, G. A. Covic and J. T. Boys, “An approximate dynamic model of LCL-T-based inductive power transfer power supplies,” *IEEE Transactions on Power Electronics*, vol. 29, no. 10, pp. 5554–5567, 2014.

[15] J. Zhao, Z. Zhang and Y. Xing, “Design and implementation of double-sided LCL variable compensation topology of MCR-WPT system,” *IEEJ Transactions on Electrical and Electronic Engineering*, vol. 15, no. 12, pp. 1853–1862, 2020.

[16] L. Tan, M. Zhang, S. Wang, S. Pan, Z. Zhang *et al.,* “The design and optimization of a wireless power transfer system allowing random access for multiple loads,” *Energies*, vol. 12, no. 6, pp. 1017, 2019.

[17] Z. Pantic, S. Bai and S. M. Lukic, “ZCS LCC-compensated resonant inverter for inductive-power-transfer application,” *IEEE Transactions on Industrial Electronics*, vol. 58, no. 8, pp. 3500–3510, 2011.

[18] S. Li, W. Li, J. Deng, T. D. Nguyen and C. C. Mi, “A double-sided LCC compensation network and its tuning method for wireless power transfer,” *IEEE Transactions on Vehicular Technology*, vol. 64, no. 6, pp. 2261–2273, 2015.

[19] W. Li, H. Zhao, J. Deng, S. Li and C. C. Mi, “Comparison study on SS and double-sided LCC compensation topologies for EV/PHEV wireless chargers,” *IEEE Transactions on Vehicular Technology*, vol. 65, no. 6, pp. 4429–4439, 2015.

[20] C. Liu, S. Ge, Y. Guo, H. Li and G. Cai, “Double-LCL resonant compensation network for electric vehicles wireless power transfer: Experimental study and analysis,” *IET Power Electronics*, vol. 9, no. 11, pp. 2262–2270, 2016.

[22] Y. Yao, Y. Wang, X. Liu, F. Lin and D. Xu, "A novel parameter tuning method for a double-sided LCL compensated WPT system with better comprehensive performance," *IEEE Transactions on Power Electronics*, vol. 33, no. 10, pp. 8525–8536, 2018.

[23] Y. Xiao, C. Liu, Y. Huang and S. Liu, "Concurrent wireless power transfer to multiple receivers with additional resonant frequencies and reduced power switches," *IEEE Transactions on Industrial Electronics*, vol. 67, no. 11, pp. 9292–9301, 2019.

[24] M. Rozman, A. Ikpehai, B. Adebisi, K. M. Rabie, H. Gacanin *et al.,* "Smart wireless power transmission system for autonomous EV charging," *IEEE Access*, vol. 7, pp. 112240–112248, 2019.

[25] T. A. Huynh and M. F. Hsieh, "Performance analysis of permanent magnet motors for electric vehicles (EV) traction considering driving cycles," *Energies*, vol. 11, no. 6, pp. 1385, 2018.

[26] A. Koran and K. Badran, "Adaptive frequency control of a sensorless-receiver inductive wireless power transfer system based on mixed-compensation topology," *IEEE Transactions on Power Electronics*, vol. 36, no. 1, pp. 978–990, 2020.

[27] A. Kamalaselvan and S. L. Prakash, "Modeling simulation and analysis of closed loop speed control of PMSM drive system," in *Proc. Int. Conf. on Circuits, Power and Computing Technologies*, Nagercoil, India, pp. 692–697, 2014.

[28] S. Li, W. Li, J. Deng, T. D. Nguyen and C. C. Mi, "A double-sided LCC compensation network and its tuning method for wireless power transfer," *IEEE Transactions on Vehicular Technology*, vol. 64, no. 6, pp. 2261–2273, 2014.

[29] P. Pillay and R. Krishnan, "Modeling of permanent magnet motor drives," in *IECON'87: Motor Control and Power Electronics*, Cambridge, MA, pp. 289–293, 1987.

[30] H. Feng, T. Cai, S. Duan, J. Zhao, X. Zhang *et al.,* "An LCC-compensated resonant converter optimized for robust reaction to large coupling variation in dynamic wireless power transfer," *IEEE Transactions on Industrial Electronics*, vol. 63, no. 10, pp. 6591–6601, 2016.

[31] L. Robert, "A comparison of half-bridge resonant converter topologies," *IEEE Transactions on Power Electronics*, vol. 3, no. 2, pp. 174–182, 1988.

[32] W. Zhang and C. C. Mi, "Compensation topologies of high-power wireless power transfer systems," *IEEE Transactions on Vehicular Technology*, vol. 65, no. 6, pp. 4768–4778, 2015.

[33] D. B. Kshatri, S. Shrestha and B. Shrestha, "A brief overview of wireless power transfer techniques," *International Journal of Advanced Smart Convergence*, vol. 4, no. 2, pp. 1–5, 2015.